Tectonophysics 878 (2024) 230300

Contents lists available at ScienceDirect

Tectonophysics

journal homepage: www.elsevier.com/locate/tecto

Structure and dynamics of southern Mariana margin: Constraints from seismicity, tomography and focal mechanisms

Xinyang Wang [a], Shaohong Xia [a,d,*], Hongfeng Yang [b,e], Han Chen [b], Dapeng Zhao [c]

[a] CAS Key Laboratory of Ocean and Marginal Sea Geology, South China Sea Institute of Oceanology, Chinese Academy of Sciences, Guangzhou 510301, China
[b] Earth and Environmental Sciences Programme, Faculty of Science, The Chinese University of Hong Kong, Hong Kong, China
[c] Department of Geophysics, Graduate School of Science, Tohoku University, Sendai 980-8578, Japan
[d] Southern Marine Science and Engineering Guangdong Laboratory (Guangzhou), Guangzhou 511458, China
[e] Shenzhen Research Institute, The Chinese University of Hong Kong, Shenzhen, China

ARTICLE INFO

Keywords:
Southern Mariana margin
Seismic tomography
Subduction zone
Geodynamic evolution
Magmatism
Arc lower crustal foundering

ABSTRACT

The southern Mariana margin is a tectonically distinctive and rapidly deforming region with the world deepest trench and unusual deformation and magmatism. However, its related deep structure and dynamics are still poorly understood. In this study, we determine robust 3-D P and S wave velocity models down to 130 km depth beneath the southern Mariana margin by using arrival-time data of local earthquakes recorded at 12 near-field seismic stations. Our tomographic results together with local seismicity and focal mechanisms reveal that the subducted Pacific slab is rapidly rolling back with a steep dip angle and narrowly but strongly coupled with the thin forearc block, which results in the deepest trench. An inferred eastward mantle flow transports the enhanced hydrous mantle melt beneath the southwest Mariana rift to the southern Mariana Trough, causing unusual deformation, magmatism and volcanism in the new oceanic crust. In addition, seismicity in the west Mariana ridge lithosphere may indicate active foundering of the arc lower crust.

1. Introduction

The southern Mariana convergent margin (Fig. 1) terminates the ~1500 km-long classic Mariana-type trench/arc/back-arc subduction system and evolves into a tectonically complex and rapidly deforming region (e.g., Martinez et al., 2000; Fryer et al., 2003; Gvirtzman and Stern, 2004; Stern et al., 2013). The old Pacific plate (~140–150 Ma) is subducting beneath the young Philippine Sea plate (PSP) at a rate of ~3 cm/yr (Bird, 2003) there, resulting in not only the development of an ultra-deep trench segment (including the Challenger Deep, 10,920 m) but also the formation of new oceanic crust with unusual magmatic crustal accretions (Stern et al., 2014; Martinez et al., 2018), tectonic deformation (Fryer et al., 2003; Ribeiro et al., 2013a, 2013b, 2015; Martinez et al., 2018) and submarine arc volcanism (Stern et al., 2013; Brounce et al., 2016; Ribeiro et al., 2020). Focused and diffused modes of extension and crustal accretion are both vigorously occurring within the southern Mariana Trough (Martinez et al., 2018). The former is accomplished by seafloor spreading along the Malaguana–Gadao Ridge (MGR) and accreted to the rigid PSP to the northwest (Stern et al., 2013; Martinez et al., 2018). However, the latter is trench-parallelly diffusely extended in the southeast of the ridge, forming a pervasive volcano-tectonic fabric (Martinez et al., 2018). The narrow inflated MGR also evolves into a broader diffuse spreading zone (DSZ) before moving westward to the less-opening Southwest Mariana Rift (SWMR) (Martinez et al., 2018). Earthquakes with extensional mechanisms occur actively at the northern flank of the SWMR (Zhu et al., 2019).

Juvenile arc volcanism (< 5 Ma) has emerged on the newly spread oceanic crust of the southern Mariana Trough (e.g., Stern et al., 2013; Brounce et al., 2016; Ribeiro et al., 2020) and brought up a string of small special arc volcanoes known as the Fina Nagu Volcanic Chain (Brounce et al., 2016) and the Alphabet seamounts (Stern et al., 2013). These volcanoes align linearly east of and running sub-parallel to the MGR and progress younger toward the northeast with the northernmost ones being recently active (Stern et al., 2013; Brounce et al., 2016). In contrast with the stable arc stratovolcanoes to the north (Calvert et al., 2008; Takahashi et al., 2007), they are composed of small, closely spaced submarine volcanic cones and calderas (Stern et al., 2013; Brounce et al., 2016; Ribeiro et al., 2020). Different from the mature arc

* Corresponding author at: CAS Key Laboratory of Ocean and Marginal Sea Geology, South China Sea Institute of Oceanology, Chinese Academy of Sciences, Guangzhou 510301, China.
E-mail address: shxia@scsio.ac.cn (S. Xia).

https://doi.org/10.1016/j.tecto.2024.230300
Received 21 October 2023; Received in revised form 26 March 2024; Accepted 28 March 2024
Available online 30 March 2024

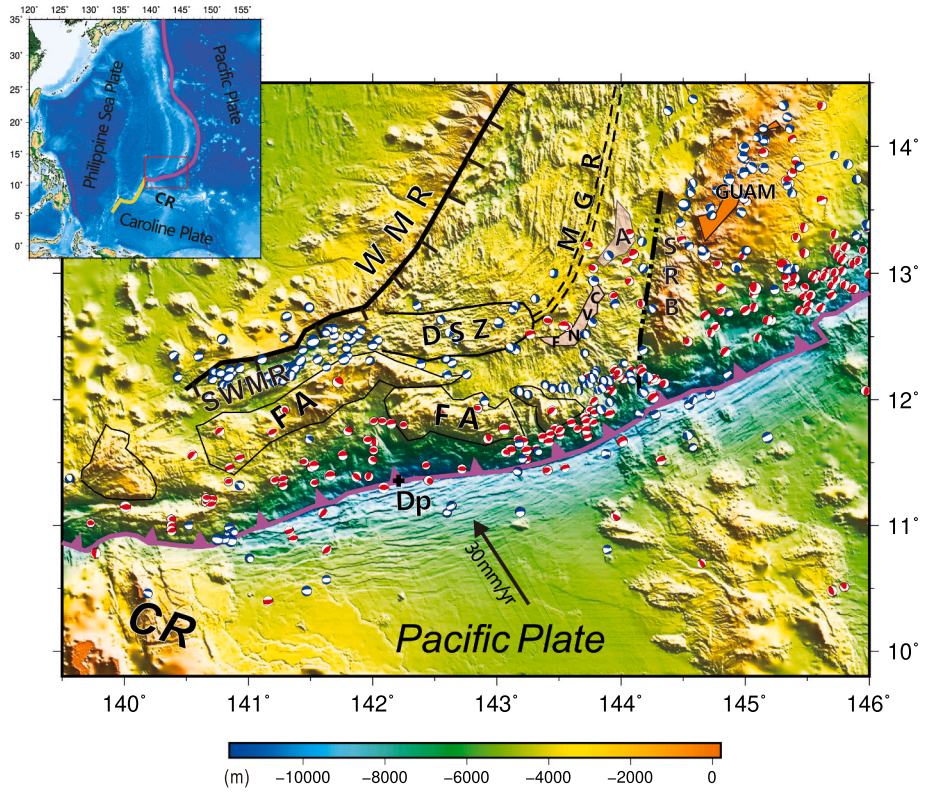

Fig. 1. Tectonic setting of the southern Mariana margin. The purple sawtooth line denotes the trench. The black arrow shows the convergence of the Pacific Plate. Red and blue beach balls denote thrust and normal fault plane solutions, respectively, from the International Seismological Center online bulletin. The black dot-dashed line denotes the West Santa Rosa Bank transform fault. SRB: the Santa Rosa Bank; CR: the Caroling ridge; Dp: the Challenger Deep. FA: the forearc block. SWMR: the Southwest Mariana Rift. DSZ: the diffuse spreading zone. WMR: the West Mariana Ridge. MGR: the Malaguana-Gadao Ridge. FNVC: the Fina Nagu Volcanic Chain. A: the Alphabet volcanos. The inset map shows location of the study area (red frame). On the inset map, the purple line shows the Izu-Bonin-Marianas trench and the yellow line shows the Yap-Palau trench. (For interpretation of the references to colour in this figure legend, the reader is referred to the web version of this article.)

magma composition ranging from water-rich basalts to rhyolites (Lee and Bachmann, 2014; Ribeiro et al., 2020), the local juvenile arc magmas are low-K basaltic to andesitic and appear as diapir-like sources of arc melts with characteristics of both back-arc and arc lavas in major and trace elements (Stern et al., 2013; Brounce et al., 2016). Furthermore, the Pliocene, low-K basaltic to basaltic andesite lavas are also discovered in the forearc rift, compositionally similar to arc lavas and back-arc basin (BAB) lavas (Ribeiro et al., 2013a, 2013b). These lavas erupted unusually close (< 80 km) to the forearc near the trench (Ribeiro et al., 2017; Stern et al., 2014), where it should be underlain by cold and dry serpentinized mantle (e.g., Hyndman and Peacock, 2003; Ohara and Ishii, 1998; Abers et al., 2017; Zhao et al., 2022). Widespread and ultra-deep plate-bending faults have been revealed in the outer rise area at the southern Mariana margin (Zhou et al., 2015; Zhou and Lin, 2018; Zhang et al., 2021; Chen et al., 2022; Zhang et al., 2023), which will cause a large amount of water input (Cai et al., 2018; Zhu et al., 2021) to hydrate and melt the mantle wedge subsequently (Kelley et al., 2006, 2010; Gou et al., 2018). Extensive mantle hydration and serpentinization have occurred in the uppermost mantle of both the subducting and overriding plates at shallow depths (Wan et al., 2019; Zhu et al., 2021; He et al., 2023). Moreover, the local magma supply has spawned a relatively thicker oceanic crust (with a thickness of ~6.3 km) than that of the central Mariana Trough to the north (crustal thickness of ~4.9 km) (Kitada et al., 2006; Martinez et al., 2018).

The unusual deformation and magmatism indicate that complex subduction zone processes are taking place there. The contemporaneous and widely distributed magmatic crustal accretion and the incipient island arc formation make this area an active analog for subduction zone infancy (Martinez et al., 2018; Ribeiro et al., 2020). The local seismicity reveals that the subducted Pacific slab at the southern Mariana margin is short (< 250 km depth) and couples unusually narrow with the overlying lithosphere (~50 km wide) (Fryer et al., 2003; Gvirtzman and Stern, 2004; Miller et al., 2006) with a relatively gentle dip (~18°) at the shallow depth (Zhu et al., 2019; Hayes et al., 2018) and a steeper dip (~29°-34°) at 150–200 km depths (Gvirtzman and Stern, 2004; Miller et al., 2004, 2006). Two pieces of evidence show that a slab tear occurs somewhere beneath the Santa Rosa Bank (Fryer et al., 2003; Gvirtzman and Stern, 2004). The first is that the Mariana Ridge is sharply terminated immediately southwest of Guam, and two large N-S striking left-lateral fault zones have developed in the west and east of the Santa Rosa Bank. The second is that the Wadati-Benioff seismic zone is disrupted and the relocated earthquakes define a steeper slab dip west of the Santa Rosa Bank than to the east. The tear can release a small slab fragment from the rest of the northern subducting plate, allowing it to independently roll back more easily (Fryer et al., 2003; Gvirtzman and Stern, 2004). However, due to the paucity of local seismic observations, the detailed deep structure and kinematics of the subducting plate and its interactions with adjacent tectonic units there are still poorly understood, which is the first-order dynamic basis to control and affect the local magmatic and tectonic evolution. In this study, we use a new travel-time data set and an earthquake catalog recorded at 12 local stations to determine 3-D seismic velocity models of the southern Mariana region. Combining the tomographic results with the local seismicity and focal mechanisms, we aim to better understand the geodynamic processes in the study region.

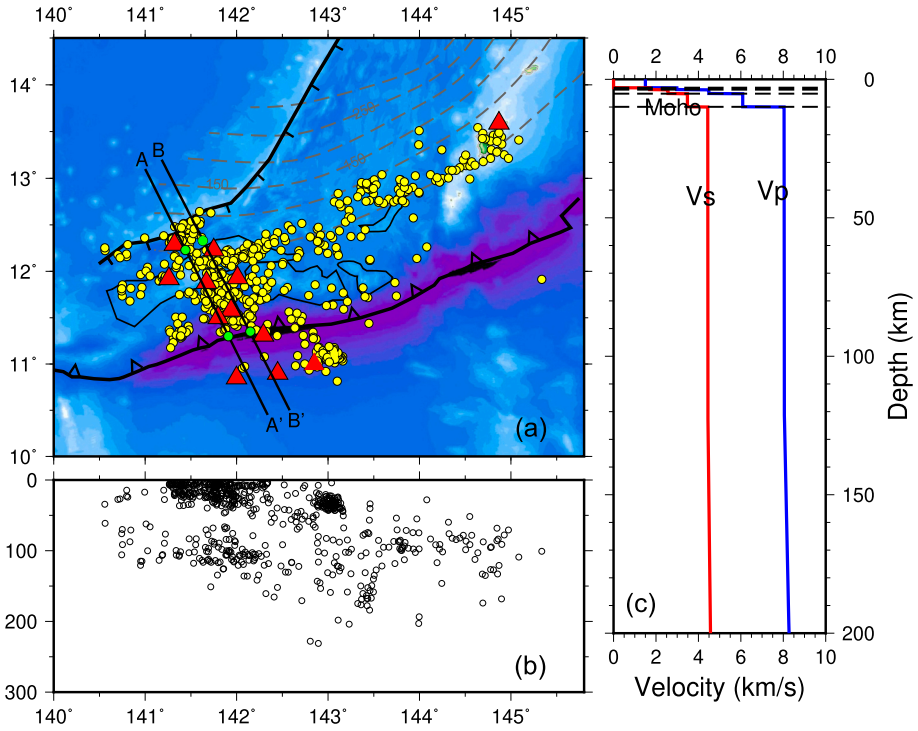

Fig. 2. (a) Epicentral distribution of the 665 local earthquakes (yellow dots) and 12 seismic stations (red triangles) used in this study. The 12 stations consist of 11 Ocean Bottom Seismographs and the GUMO land-based station. The black lines A-A' and B-B′ denote locations of two vertical cross-sections shown in Fig. 7. The green dots mark locations of the SWMR and the trench at each profile. (b) East-west vertical cross-sections of the earthquakes shown in (a). (c) The 1-D velocity model used in this study. Red and blue lines represent the S-wave and P-wave velocities, respectively. (For interpretation of the references to colour in this figure legend, the reader is referred to the web version of this article.)

2. Data and method

Our arrival time data of local earthquakes were recorded at 11 near-field ocean-bottom-seismograph (OBS) stations deployed in and around the southern Mariana margin, together with the GUMO land station during December 2016 to June 2017 (Zhu et al., 2019; Chen et al., 2022) (Fig. 2). Although a large number of local earthquakes were detected during the experiments (Zhu et al., 2019; Chen et al., 2022), only 665 well-located local earthquakes are selected to conduct tomographic inversion based on the following criteria: (1) each event is relocated using all the P- and S-wave arrival times taking into account the surface topography and velocity discontinuities (Zhao et al., 1992), and only the events with uncertainties <20 km in focal depth, 15 km in epicentral location are used (Fig. S1); (2) the travel-time residual of each arrival is <2.5 s (Fig. S2) and each event has six or more arrivals. As a result, a total of 5058 P-wave and 4038 S-wave arrivals are used to determine 3-D P- and S-wave velocity (Vp, Vs) models. The employed stations and earthquakes are distributed over the WMR, the SWMR, forearc and outer-rise areas. In addition, focal mechanism solutions from the International Seismological Center online bulletin are compiled to constrain the strain field (Dziewonski et al., 1981; Ekström et al., 2012).

The tomography method of Zhao et al. (1992) is applied to determine the 3-D Vp and Vs models of the study region. The same 1-D local Vp model as Zhu et al. (2019) is taken as the starting model, which is derived from the CRUST1.0 model (Laske et al., 2013) and a 2-D crustal Vp model (Wan et al., 2019). The mantle velocity follows the IASP91 Earth model (Kennett and Engdahl, 1991). The 1-D Vs model is estimated from the Vp model by assuming a Vp/Vs ratio of 1.75 in the crust and 1.81 in the upper mantle (Zhu et al., 2019). The station elevations and constant depths of the sediment basement (0.71 km), the Conrad (2.18 km) and Moho discontinuities (6.93 km) underneath the surface topography (Zhu et al., 2019) are taken into account in the 3-D ray tracing. A least-squares algorithm with damping and smoothing regularizations is used to solve the large but sparse system of observation equations (Zhao et al., 1992; Wang et al., 2017; Jia and Zhao, 2023). A 3-D grid is set up in the modeling space to express the 3-D velocity structure with a lateral grid interval of 0.3° (~30 km). The vertical grid meshes are set at depths of 8, 16, 24, 32, 46, 60, 80, 100, 130, and 160 km.

Checkerboard resolution tests (CRTs) are performed to evaluate the rationality of the grid settings and the resolution of the tomographic models (Zhao et al., 1992, 2012). In the CRTs, we first construct a 3-D checkerboard model with alternative positive and negative velocity anomalies (4%) assigned to the grid nodes. Then we calculate synthetic travel times with the same set of source-receiver paths as those in the real data set based on the checkerboard model. Then the synthetic data are inverted by using the same starting velocity model and inversion algorithm to produce a recovered image of the input checkerboard model. The resolution is considered to be good in areas where the checkerboard pattern is recovered well. The test results show that at 8 km depth slice the checkerboard pattern is recovered well but just in the area covered by seismic stations (Figs. 3 and 4). As the depth increases, the recovered area increases and expands to the Guam island. The Vp and Vs CRT results show a similar pattern, indicating that we can obtain robust 3-D Vp and Vs images beneath the southern Mariana margin. The CRT results also demonstrate that the obtained tomographic images generally have good resolution for the grid setting. More CRT results are shown in Figs. S3–S6.

3. Results

Figures 5 and 6 show map views of the obtained Vp and Vs images, respectively, together with the focal mechanisms and the used local earthquakes. In the tomographic results, the distribution of prominent anomalies accords well with the local geological features at shallow depths. At depths of 8 km (Figs. 5a and 6a) and 16 km (Figs. 5b and 6b),

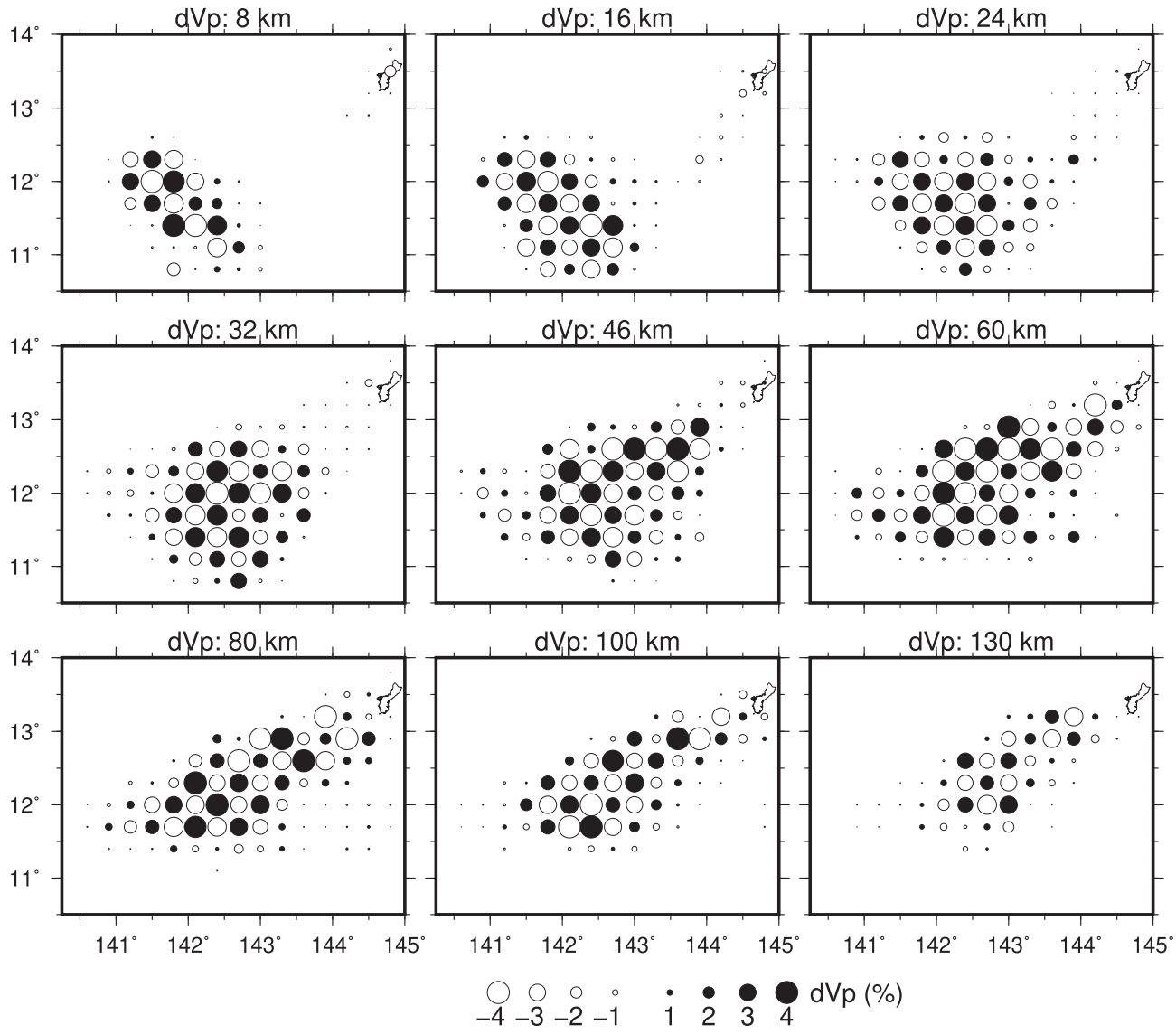

Fig. 3. Results of a checkerboard resolution test for Vp tomography at depths of 8 km to 130 km. The layer depth is shown above each map. The black and white circles denote high and low Vp perturbations, respectively, whose scale is shown at the bottom.

the SWMR is revealed as a distinct low-velocity (low-V, i.e. low-Vp and low-Vs) anomaly and sandwiched between two high-velocity (high-V, i.e. high-Vp and high-Vs) anomalies. The two high-V anomalies represent the forearc block facing the challenger deep and the WMR, respectively. The SWMR is an outlet of the mantle melts which absorbed abundant slab-derived fluids (e.g., Grove et al., 2006). As a result, the mantle wedge beneath the SWMR shows low-velocity. By comparison, the WMR and the forearc block are from a remnant Miocene arc, experiencing creation, growth accretion of initial mafic arc crust from mantle-derived primary basaltic magma and somewhat magmatic differentiation (Takahashi et al., 2007, 2008; Tatsumi et al., 2008). Thus, they show high-velocity. At the front of the SWMR, the subducting Pacific plate is revealed as a high-V anomaly. A remarkable feature appears in the outer-rise area, where two prominent anomalies are imaged adjacent to each other but with opposite velocity perturbations, which may be related to the crustal or lithospheric nature (Xu et al., 2023). Among them, the prominent low-V anomaly in the outer-rise area is consistent with the result of Rayleigh wave tomography (Zhu et al., 2021), which may reflect the incoming plate hydration (e.g., Cai et al., 2018; Zhu et al., 2021; Yu and Zhao, 2020; Zhao et al., 2022). Also, a cluster of earthquakes related to the plate-bending (Chen et al., 2022) occurs in the outer-rise low-V anomaly down to 50 km depth (Figs. 5e and 6e). However, the significant velocity variations revealed within the supposedly uniform and thick 150-Myr-old lithosphere of the Pacific plate in that region highlight the need for further observations and studies. As the depth increases from 24 km (Figs. 5c and 6c), the subducted high-V Pacific slab advances northwestward and the high-V WMR lithospheric anomaly shrinks to vanish. Earthquakes with thrust mechanisms mostly appear along the subducted slab front at a depth of 16 km (Figs. 5b and 6b). Plentiful extensional earthquakes occurred at the edge between the high-V WMR and the low-V SWMR, with a maximum depth of $<$40 km (Figs. 5d and 6d). The distribution of the local seismicity also shows that many earthquakes occurred in the high-V WMR. At depths of 80 km (Figs. 5g and 6g) and 100 km (Figs. 5h and 6h), the imaged subducted slab presents relatively good continuity and some intermediate-depth earthquakes occurred along it.

Figure 7 shows two vertical Vp and Vs cross-sections at the southernmost Mariana margin (more profiles are shown in Figs. S7–S9). The

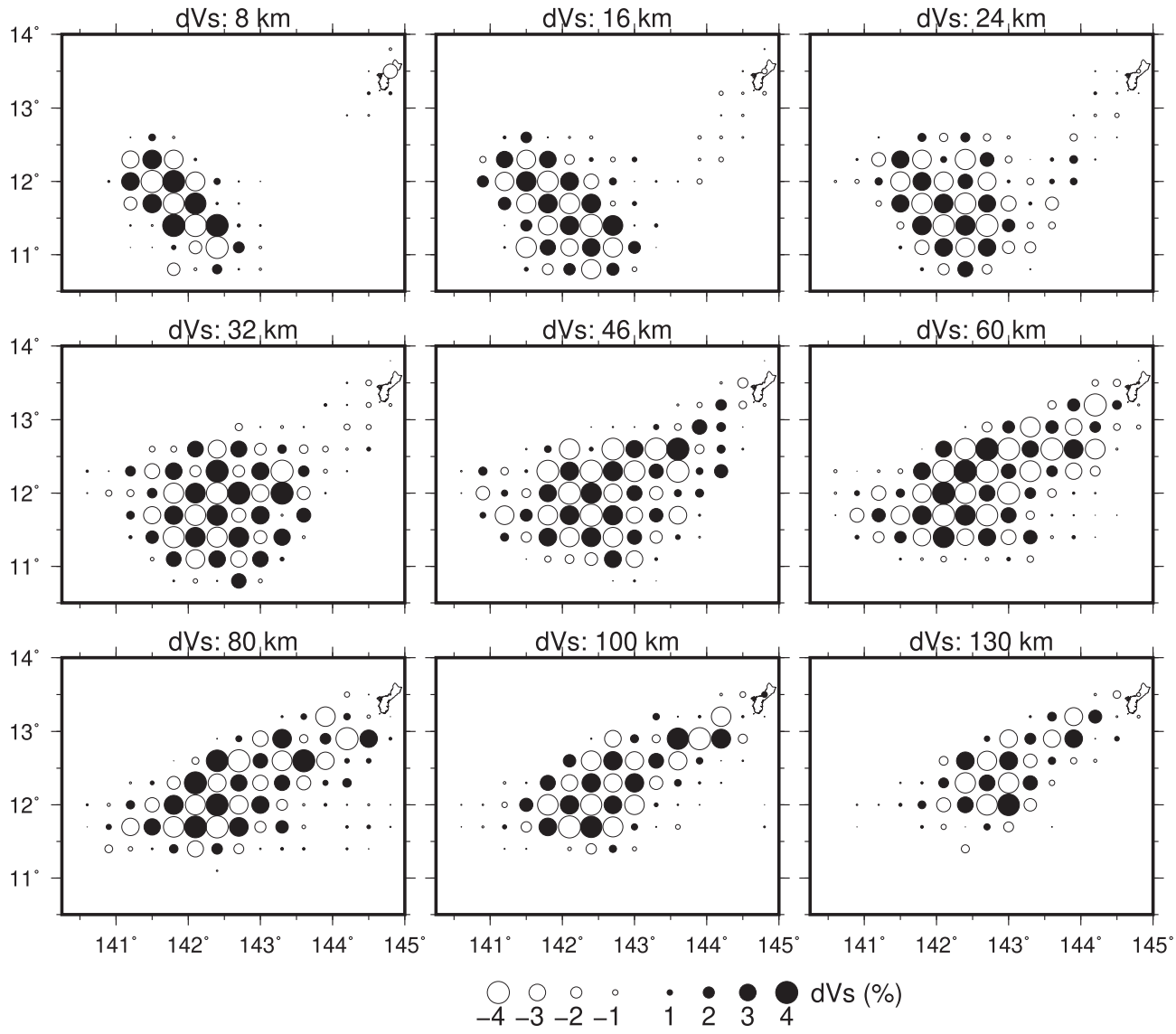

Fig. 4. The same as Fig. 3 but for Vs tomography.

profiles roughly pass through the OBS sites, where the tomography has a good resolution. Local earthquakes and focal mechanism solutions within a 6-km width are projected onto each profile. In the images, the subducting Pacific slab is clearly imaged as a dipping high-V anomaly. The A-A' Vp profile clearly shows a high-Vp anomaly with a thickness of ~30 km in the forearc block, coupled with the slab at its leading edge. Moreover, a high-V anomaly with a thickness of ~50 km is revealed beneath the WMR in both Vp and Vs images. Some detected earthquakes and normal-faulting events occurred in and around the high-V WMR anomaly. In the mantle wedge, a prominent low-V anomaly appears above the high-V slab, and close to the high-V forearc and the high-V WMR. Based on our tomography combined with the distribution of local earthquakes and focal mechanism solutions, we outline a new upper surface of the subducted slab. The newly estimated slab interface shows that the subducted slab actually has a steep dip, ~40° at the shallow depth and steeper in the deeper part, similar to the previous results (Gvirtzman and Stern, 2004; Hayes et al., 2012; Zhou and Lin, 2018; Li et al., 2023) but considerably different from the Slab2.0 model (Hayes et al., 2018; Zhu et al., 2019). Additional profiles, depicted in Figs. S8 and S9, provide further insights into the northward changes in the morphology of the subducted slab. These profiles show that the slab interface fit between the Slab2.0 model and our tomographic results becomes better to the north, and the slab becomes steeper at greater depths. In the A-A' profile, some earthquakes are located in the high-V Pacific slab at depths of ~30–60 km, which occurred as a line trend approximately normal to the plate dip angle. Meanwhile, two thrust-faulting events are located at the bottom of the high-V slab in the A-A' profile.

To evaluate the robustness of the tomographic images, we performed restoring resolution tests (RRTs) (Zhao et al., 1992, 2012). The RRT procedure is the same as that of the CRT but the input model is different. The RRT input model is derived from the main features of the tomographic results to test the smearing effect and the resolvability of the major features, especially for the areas where the CRT does not show a good result (Zhao et al., 1992, 2012). The RRT results show that the characteristic anomalies reflecting the high-V slab and low-V mantle wedge are well recovered (Fig. 8). However, due to the sparse ray coverage at the seismic array edge, the high-V WMR anomaly is recovered incompletely, with a reduced anomaly volume and amplitude. While this incomplete restoration may affect its bulk but not the

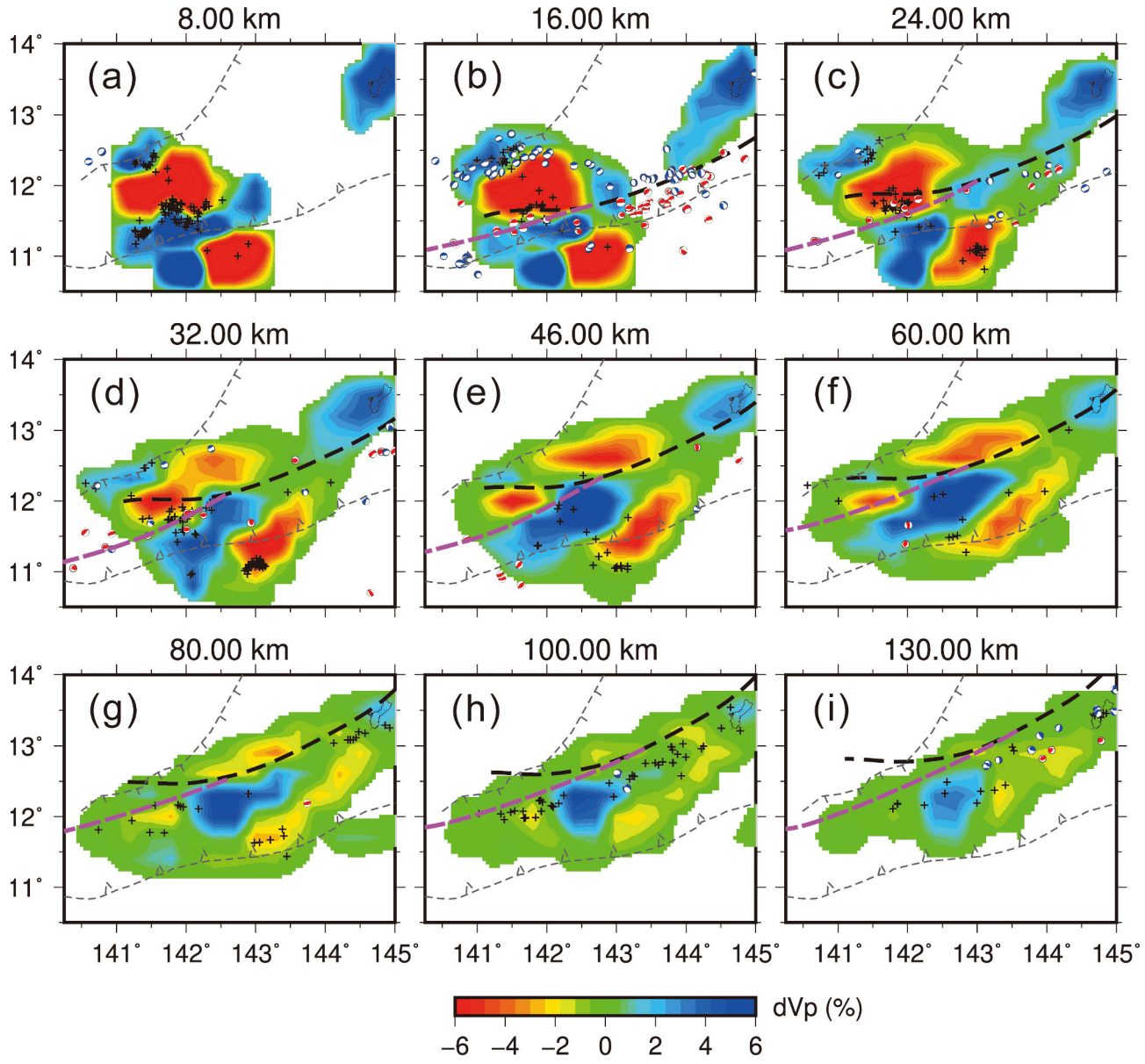

Fig. 5. Map views of the obtained Vp tomography. The layer depth is shown above each map. The red and blue colors denote low and high Vp perturbations, respectively, whose scale is shown at the bottom. The comb dashed line denotes the West Mariana Ridge; the sawtooth dashed line denotes the southern Mariana trench. In (b-i), the black dashed line denotes location of the Pacific slab upper boundary at each depth from the Slab2.0 model (Hayes et al., 2018), whereas the purple dashed line denotes newly estimated location of the slab upper boundary. In (a) and (b), the local earthquakes (crosses) and focal mechanisms within a depth range of 4 km are plotted, whereas the range is 5 km in (c-i). Red and blue beach balls denote thrust and normal fault plane solutions, respectively. (For interpretation of the references to colour in this figure legend, the reader is referred to the web version of this article.)

reliability of its existence. Thus, the RRT tests demonstrate that the major velocity anomalies in the images are reliable.

4. Discussion

Our tomographic images reveal the 3-D upper-mantle structure (<130 km depth) of the southern Mariana margin, which provide important constraints on local seismotectonics, magmatism and deformation.

4.1. Tectonic cause of the deepest trench

Our tomographic results reveal the steep dip angle of the subducted Pacific slab and its changes with depth at the southern Mariana margin, nearly 40° in the shallow areas and steeper with depth, which well characterizes the slab flexural bending shape. The increasing dip angle with depth reflects the strong flexure and rapid rollback of the subducted slab (Zhou et al., 2015; Zhang et al., 2018). The earthquakes linearly taking place in the subducted slab at 30–60 km depths in the A-A' profile appear to occur as a result of successive ruptures of the fault, which could be triggered by the slab bending, similar to the outer-rise bending faults but at greater depths (Ivandic et al., 2008; Zhou et al., 2015; Wang et al., 2022). The strong flexural bending of the downgoing slab will reactivate the preexisting faults or create new faults, and result in the fault-related intraslab seismicity (e.g., Mishra and Zhao, 2004; Wang et al., 2023). Previous studies have speculated the local rapid slab rollback based on the modeling hypothesis that a narrow slab can roll back more rapidly than a wide slab (Dvorkin et al., 1993), the local shallow asthenosphere penetration at the top of the mantle wedge (Gvirtzman and Nur, 1999; Gvirtzman and Stern, 2004) and some field

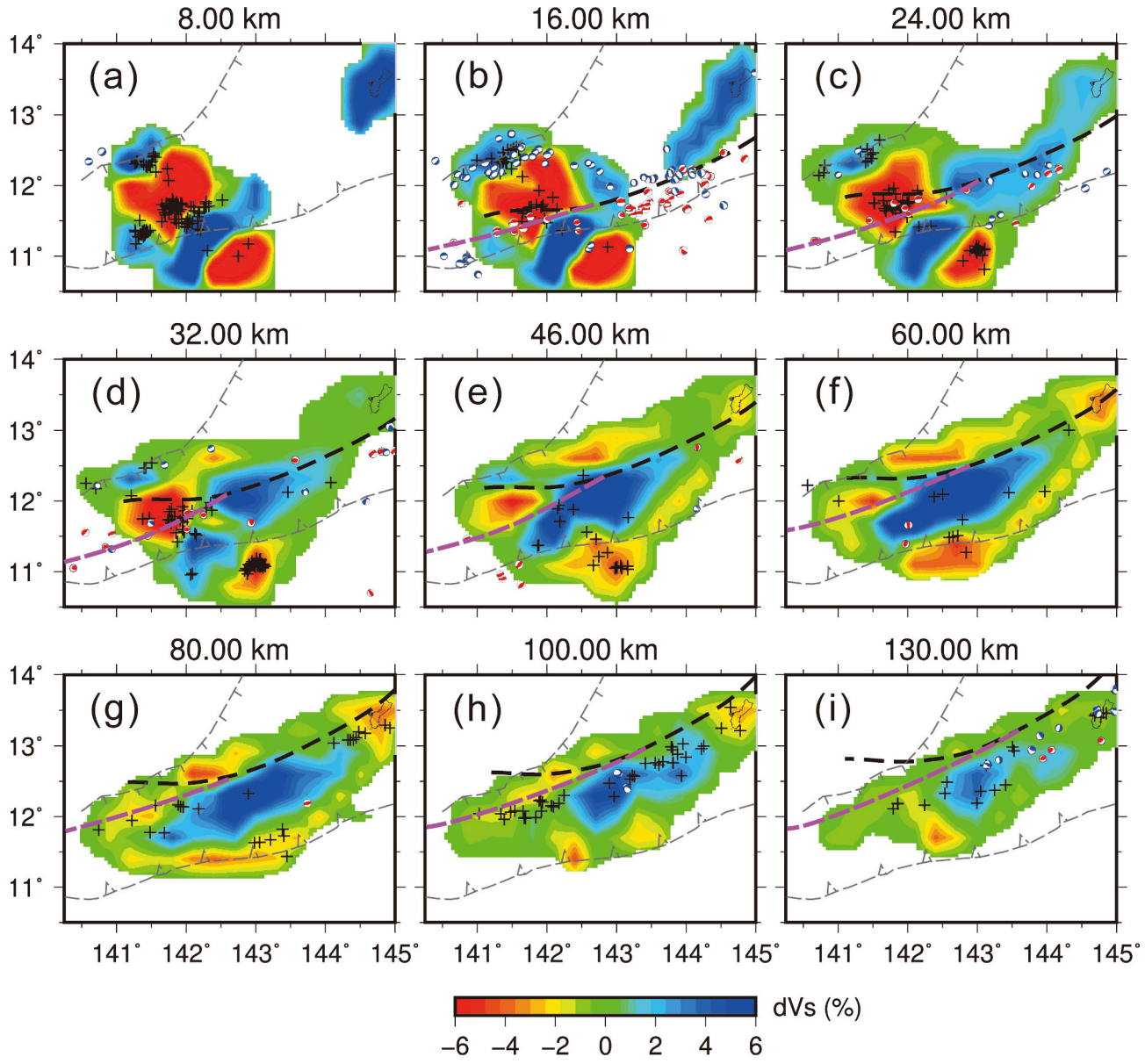

Fig. 6. The same as Fig. 5 but for Vs tomography.

observations (Fryer et al., 2003). The strong slab flexure and its deep fault-related earthquakes revealed in this study may provide direct dynamic evidence on the rapid slab rollback at the southern Mariana margin (Emry et al., 2014; Zhou et al., 2015). Comprehensively, the rapid rollback should be also facilitated by the slab tear west of the Guam separating the southern slab fragment to independently roll back (Fryer et al., 2003; Gvirtzman and Stern, 2004) and its related sideway flow eliminating the asthenospheric hydrodynamic suction to the subducting slab (Dvorkin et al., 1993; Ribeiro et al., 2017). The steep slab angle and rapid slab rollback make the bending-related faults develop into the slab and make the compressional stress beneath the neutral plane (Emry et al., 2014) large enough to generate compressional brittle faulting extending into the slab, just like the two thrust-faulting events at the bottom of the high-V slab in the A-A' profile.

Although the forearc is imaged as a thin high-V anomaly in the Vp tomography, its lithospheric thickness still cannot be well estimated due to the invasion of asthenospheric mantle and derivative hydrous melts which can reduce seismic velocity (Stern et al., 2014; Wan et al., 2019). The combined effects of extension, hydration, and melt invasion would further weaken and thin the forearc lithosphere (Stern et al., 2014). The calculated shape of the asthenospheric wedge based on the isostatic equilibrium indicates that the asthenospheric penetration at the Challenger Deep is very shallow and close to the trench (Gvirtzman and Stern, 2004), corresponding to a thin and narrow (~50 km wide) forearc, which is well imaged by our tomography. The thin forearc lithosphere and the steep slab lead to an unusually narrow interplate megathrust zone between the overlying forearc lithosphere and the subducted slab (Gvirtzman and Stern, 2004), and result in the asthenosphere penetrating shallower and closer to the trench than typical subduction zones (Gvirtzman and Stern, 2004; Stern et al., 2014). On the other hand, in southern Mariana both extensional and compressional earthquakes occur in the outer-rise area. Among them there is an exceptionally deep compressional earthquake (at 34 km depth) (Emry et al., 2014). Outer rise seismicity can closely reflect the stress state of the interplate coupled zone (Christensen and Ruff, 1983, 1988). In decoupled or weakly coupled subduction zones, the outer rise area is dominated by tensional stresses associated with plate bending and/or slab pull, where only tensional outer-rise earthquakes occur. By contrast, in the locked or strongly coupled subduction zones, compressional stress will accumulate in the outer rise from the continuous plate

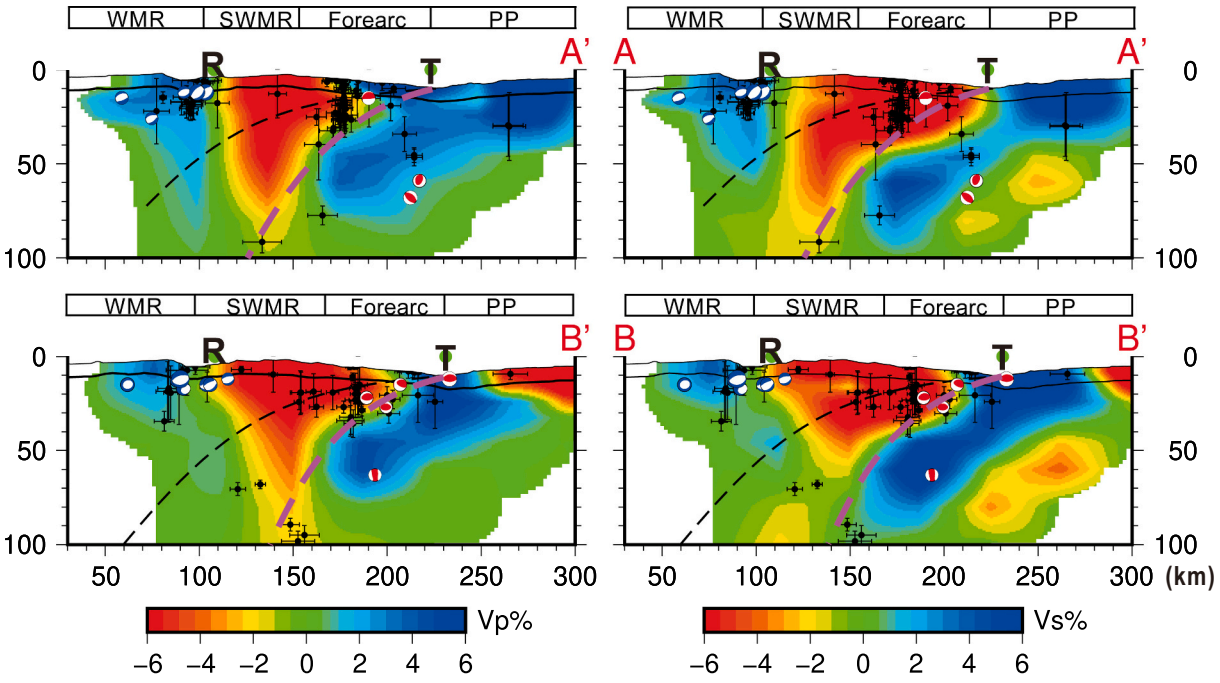

Fig. 7. Vertical cross-sections of Vp (left column) and Vs (right column) tomography along the profiles shown in Fig. 2a. The red and blue colors denote low and high velocity perturbations, respectively, whose scales are shown at the bottom. The local earthquakes with uncertainties of epicenter and focal depth (black dots with horizontal and vertical black bars) and focal mechanism solutions (beach balls) within a 6-km width of each profile are plotted. Red and blue beach balls denote thrust and normal fault plane solutions, respectively. The solid curved line denotes the Moho discontinuity. The black dashed line denotes the upper boundary of the subducting Pacific slab from the Slab2.0 model, whereas the purple dashed line denotes the newly estimated slab upper boundary based on the tomographic images and the local earthquakes. The labels T and R denote locations of the trench and the Southwest Mariana Rift, respectively. The tectonic divisions are shown above each panel. WMR: the West Mariana Ridge; SWMR: the Southwest Mariana Rift; PP: the Pacific Plate. (For interpretation of the references to colour in this figure legend, the reader is referred to the web version of this article.)

convergence, where both tensional and compressional outer-rise events occur (Christensen and Ruff, 1988). The occurrence of the deep compressional earthquake at the southern Mariana outer rise indicates an elevated neutral plane and brittle faulting in the compressional field (Emry et al., 2014), which strongly indicates that the Pacific plate in southern Mariana is undergoing significant regional compression under a strong interplate coupling (Christensen and Ruff, 1988; Emry et al., 2014). The best-fitting flexure model matching well the local extensional and compressional earthquake locations and depths also supports this point (Emry et al., 2014). Thus, the interplate coupling in southern Mariana is narrow but strong, which can further bend and pull down the leading edge of the forearc block to a lower position (Gvirtzman and Stern, 2004). These structural features may have caused the unique tectonics responsible for the formation of the deepest trench in the world.

4.2. *Unusual deformation and magmatism in the southern Mariana Trough*

Although the mantle serpentinization would dramatically reduce seismic velocity, which commonly occurs in the mantle wedge (e.g., Xia et al., 2008; Hyndman and Peacock, 2003), we speculate that the large-scale low-V anomaly in the mantle wedge should mainly reflect enhanced mantle melting beneath the southern Mariana margin (e.g., Kushiro, 1973; Katz et al., 2003; Grove et al., 2006). Compared to the Mariana forearc to the north, where many serpentinite mud volcanoes exist (Fryer et al., 1999), no mud volcano is found in the southern Mariana forearc (Ohara et al., 2012). Highly fractured outcrops of serpentinized peridotite were discovered in the southern Mariana forearc, however, which are supported by fault-controlled fluid pathways (Ohara et al., 2012). Young basaltic magmatism actively occurred in the inner wall and the forearc rift of the southern Mariana trench (Ribeiro et al., 2013a, 2013b; Stern et al., 2014; Ribeiro et al., 2015), which is unusually close to the trench and should be underlain by the cold and serpentinized mantle without melt (Abers et al., 2017). Igneous rock samples in that area have revealed their nature of partial melting of a BAB-like mantle source derived from hydrous asthenosphere (Ribeiro et al., 2013a, 2013b; Stern et al., 2014). Additionally, the samples from the MGR and DSZ also show regionally elevated mantle H_2O contents and higher extents of mantle melting (Martinez et al., 2018). All these pieces of evidence indicate the enhanced mantle melting. Of course, it is possible that a small portion of the low-V anomaly is caused by serpentinized forearc mantle (Ribeiro et al., 2013b; Wan et al., 2019; Zhu et al., 2021). In general, low-V anomalies in the mantle wedge may just present as tunnels connecting to arc volcanoes (e.g., Tamura et al., 2002; Zhao et al., 2015). However, beneath the southern Mariana margin, the low-V anomaly exists in most of the mantle wedge between the WMR and the deeply subducted slab. Mantle melting is a function of water content (Kelley et al., 2006, 2010). The enhanced melting reflects a much higher water input dehydrated from the incoming Pacific plate. At the southern Mariana margin, the significantly greater average trench relief, the maximum fault throws and ultra-deep outer-rise faults (Emry et al., 2014; Zhou and Lin, 2018; Chen et al., 2022) have been observed, which can enormously hydrate the incoming plate (Cai et al., 2018; Zhu et al., 2021; He et al., 2023). The vast volume of slab-derived fluids dehydrates at depth and rises up to hydrate the overlying mantle wedge to produce more flux melts (e.g., Tatsumi, 1986; Stern, 2002; Ribeiro et al., 2013a, 2013b). During the flux melt upwelling and transporting, the extension of the southern Mariana Trough and the forearc rift would keep the overlying lithosphere thin and cause local decompression melting of the fluxed mantle wedge (Ribeiro et al., 2013a).

Then, how is the melt transported to cause the unusual magmatic crustal accretions and submarine arc volcanism in the newly spreading oceanic crust of the southern Mariana Trough? To figure it out, we firstly

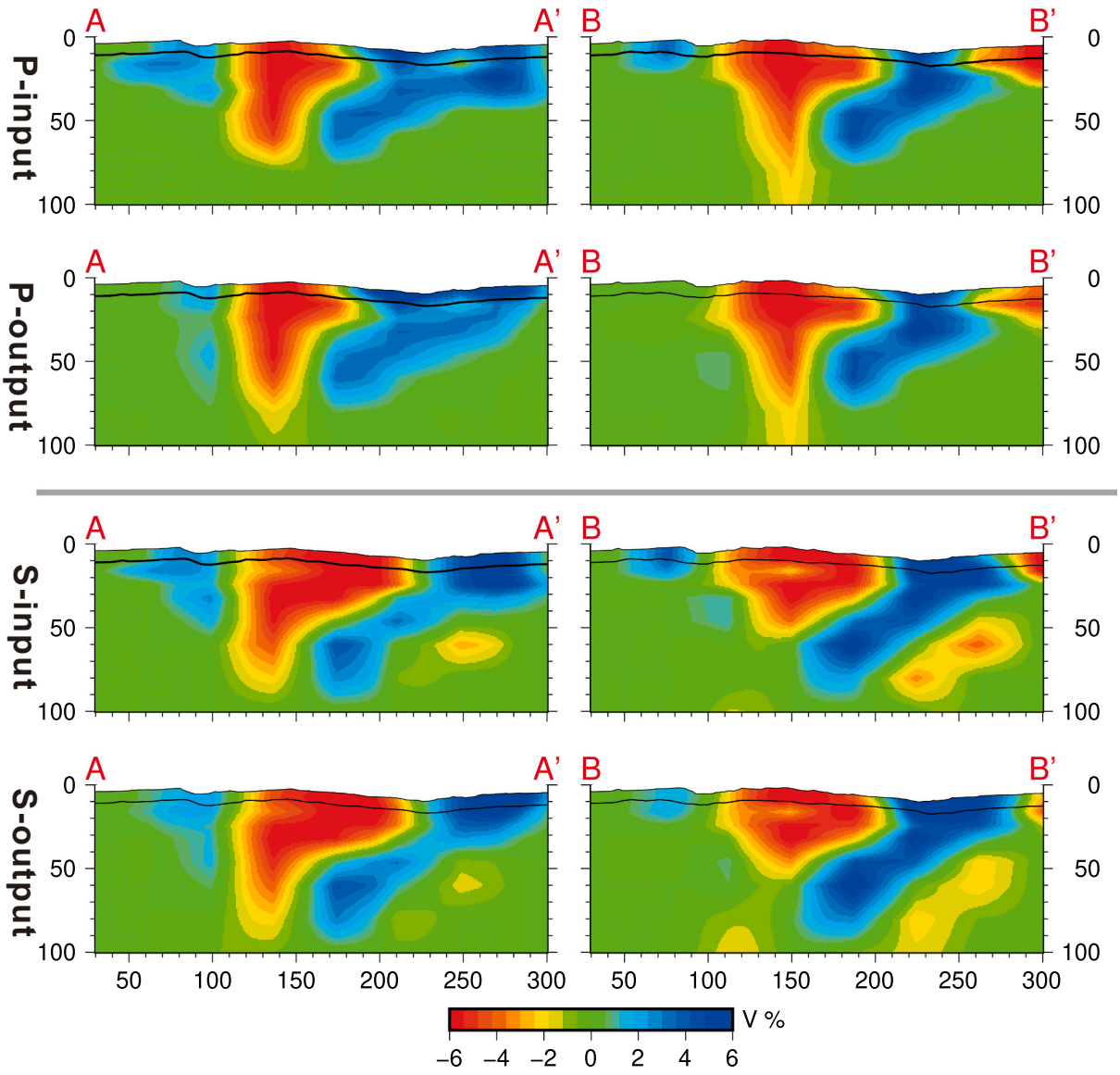

Fig. 8. Results of a synthetic test. Locations of the vertical cross-sections are shown in Fig. 2a. The labels "Input" and "Output" on the left denote the input model and output results, respectively. The red and blue colors denote low and high velocity perturbations, respectively, whose scale is shown at the bottom. (For interpretation of the references to colour in this figure legend, the reader is referred to the web version of this article.)

commence from the geological characteristics and probe into the related mantle flow. The collision with the Caroline Ridge pinned the southern termination of the Mariana arc (Miller et al., 2006) and made the Mariana trench trends nearly E-W in contrast to the more N-S orientation to the north (Gvirtzman and Stern, 2004) and prevented the back-arc extension from further extending southwestward (Wallace, 2005). The impinging Caroline Ridge and the curved subducted slab beneath southern Mariana should exert a lateral resistance on the mantle asthenosphere, which causes the upwelling mantle melt to migrate slightly eastward to the rapidly-extending southern Mariana Trough (Ribeiro et al., 2017) (Fig. 9). On the other hand, with the advancing of the Izu-Bonin-Mariana trench toward Eurasia (Carlson and Mortera-Gutiérrez, 1990; Kato et al., 2003), the PSP is shrinking in size, which squeezes out the underlying Indian-type asthenospheric mantle of the PSP to feed the southern Mariana lavas and to escape in the subducted Pacific plate through the slab tears or gaps (Ribeiro et al., 2017). The torn Caroline slab along the Sorol Trough (Fan et al., 2022) may become an outflow avenue. The slab tear southwest of Guam would be also a pathway. The eastward expansion of the low-Vp and low-Vs anomaly beneath SWMR may be a sign of the component. The asthenospheric outflow can facilitate the eastward component through the slab tear southwest of Guam. Meanwhile, the lateral component in the mantle flow and hydrodynamic shape further effectively reduce the asthenosphere suction and allow the slab to more rapidly rollback (Dvorkin et al., 1993; Gvirtzman and Stern, 2004).

Hence, we suggest that there may be an eastward component in the mantle flow that transports the subduction-related mantle magma, including the back-arc magma beneath the SWMR, eastward to the southern Mariana Trough, which results in the northeastward progression of volcanism and magmatic activities (Stern et al., 2013; Ribeiro et al., 2013a, 2013b; Brounce et al., 2016). At the same time, the eastward component mixes the mantle melts, leading to the compound lava compositions (Stern et al., 2013; Ribeiro et al., 2013a, 2013b). In this process, the change of the subduction strike, the narrow coupling zone, and the rapid slab rollback make the convecting asthenosphere to penetrate much closer to the trench (Ribeiro et al., 2013a, 2013b; Stern et al., 2014). On the other hand, subduction-related fluids and magma are abundantly generated beneath the SWMR but transported eastward to the southern Mariana Trough, which makes the SWMR less open and the narrow MGR next to the SWMR evolve into the broader DSZ

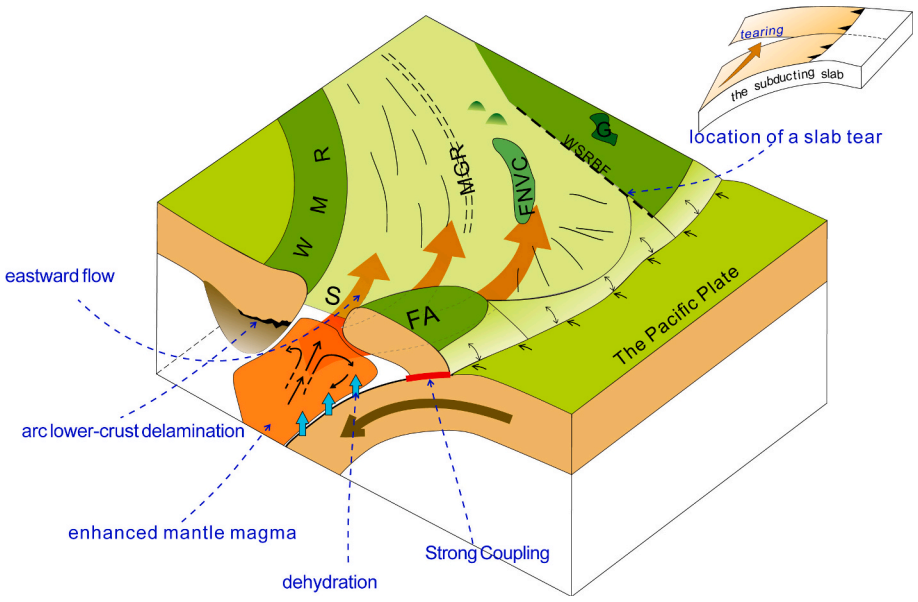

Fig. 9. A schematic diagram showing the structure and dynamics of the southern Mariana margin. S: the Southwest Mariana Rift; FA: the forearc; MGR: the Malaguana–Gadao Ridge; FNVC: the Fina Nagu Volcanic Chain; WSRBF: the west Santa Rosa Bank transform fault; G: the Guam. The large nut-brown arrow indicates the subduction of Pacific Plate. The red thick line between the forearc edge and the subducted slab indicates strong interplate coupling. The cyan arrows at the subducting slab surface indicate slab-derived fluids. The orange patch in the mantle wedge indicates hot upwelling flow. The trigeminal arrow from the enhanced mantle magma indicates eastward flow that transports the magma to the Mariana Trough. The two different brown layers beneath the WMR indicate the thick arc lithosphere whose bottom layer represents the foundering arc lower crust. The upper-right inset shows a slab tear beneath the WSRBF (Fryer et al., 2003) and the related outflow eastward across the tear (Ribeiro et al., 2017). (For interpretation of the references to colour in this figure legend, the reader is referred to the web version of this article.)

(Martinez et al., 2018). Nonetheless, volume expansion caused by the addition of subduction-related fluids still pushes the surrounding lithosphere and triggers the extensional events at the WMR lithosphere edge (Zhu et al., 2019).

4.3. An active case of arc lower crustal foundering

More attention should be paid to the active seismicity in the WMR lithosphere. The evolution of the oceanic arc crust is considered to be a primary mechanism of continental crust formation (e.g., Hamilton, 1981; Takahashi et al., 2007, 2008; Tatsumi et al., 2008). During the arc crustal growth, the mafic/ultramafic lower crustal materials can have higher density than the underlying upper mantle and become gravitationally unstable over a significant depth range of 20 to 60 km (Jull and Kelemen, 2001; Takahashi et al., 2007; Tatsumi et al., 2008; Calvert et al., 2008; Jagoutz and Behn, 2013). Then episodic foundering or delamination will seismically occur to return the mafic/ultramafic component to the mantle (Turcotte, 1989; Kay and Kay, 1993; Nakajima and Arima, 1998; Tatsumi, 2005) and ultimately result in the formation of the continental Moho (Jagoutz and Behn, 2013).

The WMR is a remnant Miocene arc with a maximum crustal thickness of ~17 km in central Mariana and ~ 9–12 km in southern Mariana, including a thick tonalitic middle crust and a thick but uneven lower crust (Takahashi et al., 2008; Wan et al., 2019). Seismic detection and petrologic modeling of central Mariana have revealed that the seismologically measured volume of the lower crust is much smaller than the petrologically inferred volume beneath the WMR, suggesting that dense lower crustal mixtures might seismically become a part of the upper mantle due to gravitational instability (Takahashi et al., 2007; Tatsumi et al., 2008). Our tomographic images reveal the thick high-V lithosphere beneath the WMR where extensional earthquakes occurred in a depth range of 10–40 km. The active seismicity in the WMR lithosphere indicates ongoing tectonic activities, which well matches the scenario of arc lower crustal foundering, i.e., the arc lower crustal rocks become gravitationally unstable over this depth range (Behn and Kelemen, 2006; Calvert et al., 2008; Jagoutz and Behn, 2013). The large difference between the seismologically and petrologically measured volumes of the lower crust, and between the oceanic island arc and the average continental crust indicates that the transfer of the lower-crustal material into the upper mantle is an important process and episodically occurs in most arcs (Takahashi et al., 2007; Tatsumi et al., 2008; Jagoutz and Behn, 2013). Similar processes have been speculated to take place in the WMR in central Mariana. In the WMR in southern Mariana, the relatively higher lower-crustal velocity than typical active island arcs (Wan et al., 2019) may reflect a denser lower crust. Based on the above discussions, we speculate a possibility that arc lower crustal foundering is occurring beneath the WMR at the southern Mariana margin. However, the foundering is triggered by the gravitational instability, but facilitated by the exerted pressure of the slab or expanding fluids in the unique tectonic setting. In southern Mariana, due to the less-opening SWMR, the subducted slab has a very short distance to the MWR. The continentward advancing slab there could transmit pressure to the MWR lithosphere directly. Meanwhile, the large amounts of fluids released from the slab could cause mantle melting and volume expansion, which could exert additional pressure.

5. Conclusions

In this study, we present robust P and S wave tomographic images of the southern Mariana margin derived from newly observed arrival-time data of local earthquakes. Our results reveal robust 3-D velocity structure of the southern Mariana margin. The tomographic images together with local seismicity and focal mechanisms offer valuable insights and important constraints on the 3-D mantle structure and subduction dynamics of the southern Mariana margin. The main findings of this work are summarized as follows.

(1) The subducted Pacific slab is rapidly rolling back with a steep dip angle and narrowly but strongly coupled with the forearc block, resulting in the world deepest trench segment in the world.

(2) Abundant slab-derived fluids are carried and released into the mantle wedge by the subducting Pacific plate, producing enhanced hydrous mantle melting. However, the enhanced magma beneath the SWMR is transported to the southern Mariana Trough by an eastward component of mantle flow, which causes the unusual deformation and magmatism there and causes less active opening of the SWMR.
(3) The seismicity in the WMR lithosphere may indicate active foundering or delamination of the arc lower crust in the southern Mariana WMR.

CRediT authorship contribution statement

Xinyang Wang: Writing – review & editing, Writing – original draft, Methodology, Funding acquisition, Formal analysis, Data curation, Conceptualization. **Shaohong Xia:** Supervision, Funding acquisition, Formal analysis, Conceptualization. **Hongfeng Yang:** Visualization, Validation, Investigation, Data curation. **Han Chen:** Validation, Investigation, Formal analysis, Data curation. **Dapeng Zhao:** Writing – review & editing, Validation, Supervision, Software, Methodology, Conceptualization.

Declaration of competing interest

The authors declare that they have no known competing financial interests or personal relationships that could have appeared to influence the work reported in this paper.

Data availability

In this work, we used the arrival-time data of local earthquakes from Zhu et al. (2019) and Chen et al. (2022), and the local earthquake catalog and the event waveform data are available online (https://academic.oup.com/gji/article/218/3/2122/5513447#137278754) and (https://doi.org/10.6084/m9.figshare.18266960.v2). The 3-D P and S wave velocity models shown in this paper and the used arrival-time data are available online (https://figshare.com/articles/dataset/3-D_Vp_and_Vs_models_of_southern_Mariana_Margin/23828397) or can be obtained by contacting the first or corresponding authors of this work.

Acknowledgments

The authors are grateful to the scientists and crew members of the R/V Shiyan-3 and the Tansuo-1 for the deployment and collection of the ocean bottom seismometer instruments. Most of the figures were made using the free GMT software (Wessel et al., 2019). We appreciate helpful discussions with Drs. Jinlong Sun, Min Xu, Kuiyuan Wan, Enyuan He, Chaoyan Fan, and Tao Gou. This work was financially supported by the Strategic Priority Research Program of the Chinese Academy of Sciences (No. XDB42020103), National Natural Science Foundation of China (42006069, 42076071, 92158205), Guangdong Key Project (No. 2019BT02H594), and Hong Kong Research Grant Council (14304820). Ling Chen (the Editor) and three anonymous referees provided thoughtful review comments and suggestions, which have improved this paper.

Appendix A. Supplementary data

Supplementary data to this article can be found online at https://doi.org/10.1016/j.tecto.2024.230300.

References

Abers, G., Van Keken, P., Hacker, B., 2017. The cold and relatively dry nature of mantle forearcs in subduction zones. Nat. Geosci. 10, 333–337. https://doi.org/10.1038/ngeo2922.
Behn, M., Kelemen, P., 2006. Stability of arc lower crust: insights from the Talkeetna arc section, south Central Alaska, and the seismic structure of modern arcs. J. Geophys. Res. 111, B11207.
Bird, P., 2003. An updated digital model of plate boundaries. Geochem. Geophys. Geosyst. 4, 1027. https://doi.org/10.1029/2001GC000252.
Brounce, M., Kelley, K., Stern, R., Martinez, F., Cottrell, E., 2016. The Fina Nagu Volcanic complex: Unusual submarine arc volcanism in the rapidly deforming southern Mariana margin. Geochem. Geophys. Geosyst. 17, 4078–4091. https://doi.org/10.1002/2016GC006457.
Cai, C., Wiens, D., Shen, W., Eimer, M., 2018. Water input into the Mariana subduction zone estimated from ocean-bottom seismic data. Nature 563, 389–392. https://doi.org/10.1038/s41586-018-0655-4.
Calvert, A., Klemperer, S., Takahashi, N., Kerr, B., 2008. Three-dimensional crustal structure of the Mariana island arc from seismic tomography. J. Geophys. Res. Solid Earth 113, 1–24. https://doi.org/10.1029/2007JB004939.
Carlson, R.L., Mortera-Gutiérrez, C.A., 1990. Subduction hinge migration along the Izu-Bonin–Mariana arc. Tectonophysics 181, 331–344.
Chen, H., Yang, H., Zhu, G., Xu, M., Lin, J., You, Q., 2022. Deep Outer-rise Faults in the Southern Mariana Subduction Zone Indicated by a Machine-Learning-based High-Resolution Earthquake catalog. Geophys. Res. Lett. 49, 1–12. https://doi.org/10.1029/2022gl097779.
Christensen, D.H., Ruff, L.J., 1983. Outer-rise earthquakes and seismic coupling. Geophys. Res. Lett. 10, 697–700.
Christensen, D.H., Ruff, L.J., 1988. Seismic coupling and outer rise earthquakes. J. Geophys. Res. 93, 13421–13444.
Dvorkin, J., Nur, A., Mavko, G., Ben-Avraham, Z., 1993. Narrow subducting slabs and the origin of backarc basins. Tectonophysics 227, 63–79. https://doi.org/10.1016/0040-1951(93)90087-Z.
Dziewonski, A.M., Chou, T.A., Woodhouse, J.H., 1981. Determination of earthquake source parameters from waveform data for studies of global and regional seismicity. J. Geophys. Res. 86, 2825–2852. https://doi.org/10.1029/JB086iB04p02825.
Ekström, G., Nettles, M., Dziewonski, A.M., 2012. The global CMT project 2004-2010: centroid-moment tensors for 13,017 earthquakes. Phys. Earth Planet. Inter. 200, 1–9. https://doi.org/10.1016/j.pepi.2012.04.002.
Emry, E.L., Wiens, D.A., Garcia-Castellanos, D., 2014. Faulting within the Pacific plate at the Mariana Trench: Implications for plate interface coupling and subduction of hydrous minerals. J. Geophys. Res. Solid Earth 119, 3076–3095. https://doi.org/10.1002/2013JB010718.
Fan, J., Zheng, H., Zhao, D., Dong, D., Bai, Y., Li, C., Zhang, Z., 2022. Seismic Structure of the Caroline Plateau-Yap Trench Collision Zone. Geophys. Res. Lett. 49, 1–10. https://doi.org/10.1029/2022gl098017.
Fryer, P., Wheat, C., Mottl, M., 1999. Mariana blueschist mud volcanism: Implications for conditions within the subduction zone. Geology 27, 103–106. https://doi.org/10.1130/0091-7613(1999)027.
Fryer, P., Becker, N., Appelgate, B., Martinez, F., Edwards, M., Fryer, G., 2003. Why is the challenger deep so deep? Earth Planet. Sci. Lett. 211, 259–269. https://doi.org/10.1016/S0012-821X(03)00202-4.
Gou, F., Kodaira, S., Kaiho, Y., Yamamoto, Y., Takahashi, T., Miura, S., Yamada, T., 2018. Controlling factor of incoming plate hydration at the North-Western Pacific margin. Nat. Commun. 9, 1–6. https://doi.org/10.1038/s41467-018-06320-z.
Grove, T.L., Chatterjee, N., Parman, S.W., Médard, E., 2006. The influence of H2O on mantle wedge melting. Earth Planet. Sci. Lett. 249, 74–89. https://doi.org/10.1016/j.epsl.2006.06.043.
Gvirtzman, Z., Nur, A., 1999. Plate detachment, asthenosphere upwelling, and topography across subduction zones. Geology 27, 563–566.
Gvirtzman, Z., Stern, R.J., 2004. Bathymetry of Mariana trench-arc system and formation of the challenger deep as a consequence of weak plate coupling. Tectonics 23, 1–15. https://doi.org/10.1029/2003TC001581.
Hamilton, W.B., 1981. Crustal evolution by arc magmatism. Philos. Trans. R. Soc. London. Ser. A. 301, 279–291.
Hayes, G.P., Wald, D.J., Johnson, R.L., 2012. Slab1.0: a three-dimensional model of global subduction zone geometries. J. Geophys. Res. 117, 180–198.
Hayes, G.P., Moore, G.L., Portner, D.E., Hearne, M., Flamme, H., Furtney, M., Smoczyk, G.M., 2018. Slab2, a comprehensive subduction zone geometry model. Science 362, 58–61.
He, E., Qiu, X., Chen, C., Wang, Y., Xu, M., Zhao, M., You, Q., 2023. Deep crustal structure across the Challenger deep: tectonic deformation and strongly serpentinized layer. Gondwana Res. 118, 135–152. https://doi.org/10.1016/j.gr.2023.02.020.
Hyndman, R., Peacock, S., 2003. Serpentinization of the forearc mantle. Earth Planet. Sci. Lett. 212, 417–432. https://doi.org/10.1016/S0012-821X(03)00263-2.
Ivandic, M., Grevemeyer, I., Berhorst, A., Flueh, E., McIntosh, K., 2008. Impact of bending related faulting on the seismic properties of the incoming oceanic plate offshore of Nicaragua. J. Geophys. Res. 113, B05410 https://doi.org/10.1029/2007JB005291.
Jagoutz, O., Behn, M., 2013. Foundering of lower island-arc crust as an explanation for the origin of the continental Moho. Nature 504, 131–134. https://doi.org/10.1038/nature12758.
Jia, R., Zhao, D., 2023. Anisotropic tomography of the East Japan subduction zone: influence of inversion algorithms. Geophys. J. Int. 234, 2199–2213. https://doi.org/10.1093/gji/ggad197.

Jull, K., Kelemen, P.B., 2001. On the conditions for lower crustal convective instability. J. Geophys. Res. 106, 6423–6446. https://doi.org/10.1029/2000JB900357.
Kato, T., Beavan, J., Matsushima, T., Kotake, Y., Camacho, J.T., Nakao, S., 2003. Geodetic evidence of back-arc spreading in the Mariana Trough. Geophys. Res. Lett. 30, 1625. https://doi.org/10.1029/2002GL016757.
Katz, R.F., Spiegelman, M., Langmuir, C.H., 2003. A new parameterization of hydrous mantle melting. Geochem. Geophys. Geosyst. 4, 1073.
Kay, R.W., Kay, S.M., 1993. Delamination and delamination magmatism. Tectonophysics 219, 177–189.
Kelley, K.A., Plank, T., Grove, T.L., Stolper, E.M., Newman, S., Hauri, E., 2006. Mantle melting as a function of water content beneath back-arc basins. J. Geophys. Res. Solid Earth 111. https://doi.org/10.1029/2005JB003732.
Kelley, K.A., Plank, T., Newman, S., Stolper, E.M., Grove, T.L., Parman, S., Hauri, E.H., 2010. Mantle melting as a function of water content beneath the Mariana arc. J. Petrol. 51, 1711–1738. https://doi.org/10.1093/petrology/egq036.
Kennett, B., Engdahl, E., 1991. Traveltimes for global earthquake location and phase identification. Geophys. J. Int. 105, 429–465.
Kitada, K., Seama, N., Yamazaki, T., Nogi, Y., Suyehiro, K., 2006. Distinct regional differences in crustal thickness along the axis of the Mariana Trough, inferred from gravity anomalies. Geochem. Geophys. Geosyst. 7, Q04011 https://doi.org/10.1029/2005GC001119.
Kushiro, I., 1973. Origins of some magmas in oceanic and circum-oceanic regions. Tectonophysics 17, 211–222.
Laske, G., Masters, G., Ma, Z., Pasyanos, M., 2013. Update on CRUST1.0—A 1-degree global model of Earth's crust. Geophys. Res. Abstr. 15, Abstract EGU2013–2658.
Lee, C.-T.A., Bachmann, O., 2014. How important is the role of crystal fractionation in making intermediate magmas? Insights from Zr and P systematics. Earth Planet. Sci. Lett. 393, 266–274.
Li, D., Chen, C., Wu, S., 2023. Local earthquake seismic tomography of the Southernmost Mariana subduction zone. Front. Earth Sci. 10, 1–10. https://doi.org/10.3389/fmars.2023.1284881.
Martinez, F., Fryer, P., Becker, N., 2000. Geophysical characteristics of the southern Mariana trough, 11°500N–13°400N. J. Geophys. Res. 105, 16591–16607. https://doi.org/10.1029/2000JB900117.
Martinez, F., Stern, R., Kelley, K., Ohara, Y., Sleeper, J., Ribeiro, J., Brounce, M., 2018. Diffuse Extension of the Southern Mariana margin. J. Geophys. Res. Solid Earth 123, 892–916. https://doi.org/10.1002/2017JB014684.
Miller, M.S., Kennett, B.L.N., Lister, G.S., 2004. Imaging changes in morphology, geometry, and physical properties of the subducting Pacific plate along the Izu-Bonin-Mariana arc. Earth Planet. Sci. Lett. 224, 363–370. https://doi.org/10.1016/j.epsl.2004.05.018.
Miller, M.S., Gorbatov, A., Kennett, B.L.N., 2006. Three-dimensional visualization of a near-vertical slab tear beneath the southern Mariana arc. Geochem. Geophys. Geosyst. 7, Q06012 https://doi.org/10.1029/2005GC001110.
Mishra, O.P., Zhao, D., 2004. Seismic evidence for dehydration embrittlement of the subducting Pacific slab. Geophys. Res. Lett. 31, L09610.
Nakajima, K., Arima, M., 1998. Melting experiments on hydrous low- K tholeiite: Implications for the genesis of tonalitic crust in the Izu-Bonin-Mariana arc. Island Arc 7, 359–373.
Ohara, Y., Ishii, T., 1998. Peridotites from the southern Mariana forearc: Heterogeneous fluid supply in mantle wedge. Island Arc 7, 541–558.
Ohara, Y., Reagan, M.K., Fujikura, K., Watanabe, H., Michibayashi, K., et al., 2012. A serpentinite-hosted ecosystem in the Southern Mariana Forearc. Proc. Natl. Acad. Sci. USA 109, 2831–2835. https://doi.org/10.1073/pnas.1112005109.
Ribeiro, J.M., Stern, R.J., Martinez, F., Ishizuka, O., Merle, S.G., Kelley, K., Anthony, E. Y., Ren, M., Ohara, Y., Reagan, M., Girard, G., Bloomer, S., 2013a. Geodynamic evolution of a forearc rift in the southernmost Mariana Arc. Island Arc 22, 453–476. https://doi.org/10.1111/iar.12039.
Ribeiro, J.M., Stern, R.J., Kelley, K.A., Martinez, F., Ishizuka, O., Manton, W.I., Ohara, Y., 2013b. Nature and distribution of slab-derived fluids and mantle sources beneath the Southeast Mariana forearc rift. Geochem. Geophys. Geosyst. 14, 4585–4607. https://doi.org/10.1002/ggge.20244.
Ribeiro, J.M., Stern, R.J., Kelley, K.A., Shaw, A.M., Martinez, F., Ohara, Y., 2015. Composition of the slab-derived fluids released beneath the Mariana forearc: evidence for shallow dehydration of the subducting plate. Earth Planet. Sci. Lett. 418, 136–148. https://doi.org/10.1016/j.epsl.2015.02.018.
Ribeiro, J.M., Stern, R.J., Martinez, F., Woodhead, J., Chen, M., Ohara, Y., 2017. Asthenospheric outflow from the shrinking Philippine Sea Plate: evidence from Hf–Nd isotopes of southern Mariana lavas. Earth Planet. Sci. Lett. 478, 258–271. https://doi.org/10.1016/j.epsl.2017.08.022.
Ribeiro, J.M., Ishizuka, O., Lee, C.A., Girard, G., 2020. Evolution and maturation of the nascent Mariana arc. Earth Planet. Sci. Lett. 530, 115912 https://doi.org/10.1016/j.epsl.2019.115912.
Stern, R., 2002. Subduction zones. Rev. Geophys. 40, 1031–1039. https://doi.org/10.1029/2001RG000108.
Stern, R., Tamura, Y., Masuda, H., Fryer, P., Martinez, F., Ishizuka, O., Bloomer, S., 2013. How the Mariana Volcanic Arc ends in the south. Island Arc 22, 133–148. https://doi.org/10.1111/iar.12008.
Stern, R., Ren, M., Kelley, K., Ohara, Y., Martinez, F., Bloomer, S., 2014. Basaltic volcaniclastics from the Challenger deep forearc segment, Mariana convergent margin: Implications for tectonics and magmatism of the southernmost Izu-Bonin-Mariana arc. Island Arc 23, 368–382. https://doi.org/10.1111/iar.12088.
Takahashi, N., Kodaira, S., Klemperer, S.L., Tatsumi, Y., Kaneda, Y., Suyehiro, K., 2007. Crustal structure and evolution of the Mariana intra-oceanic island arc. Geology 35, 203–206. https://doi.org/10.1130/G23212A.1.
Takahashi, N., Kodaira, S., Tatsumi, Y., Kaneda, Y., Suyehiro, K., 2008. Structure and growth of the Izu-Bonin-Mariana arc crust: 1. Seismic constraint on crust and mantle structure of the Mariana arc-back-arc system. J. Geophys. Res. Solid Earth 113, 1–18. https://doi.org/10.1029/2007JB005120.
Tamura, Y., Tatsumi, Y., Zhao, D., Kido, Y., Shukuno, H., 2002. Hot fingers in the mantle wedge: New insights into magma genesis in subduction zones. Earth Planet. Sci. Lett. 197, 105–116. https://doi.org/10.1016/S0012-821X(02)00465-X.
Tatsumi, Y., 1986. Formation of the volcanic front in subduction zones. Geophys. Res. Lett. 13, 717–720.
Tatsumi, Y., 2005. The subduction factory; how it operates in the evolving Earth. GSA Today 15, 4–10.
Tatsumi, Y., Shukuno, H., Tani, K., Takahashi, N., Kodaira, S., Kogiso, T., 2008. Structure and growth of the Izu-Bonin-Mariana arc crust: 2. Role of crust-mantle transformation and the transparent Moho in arc crust evolution. J. Geophys. Res. 113, B02203 https://doi.org/10.1029/2007JB005121.
Turcotte, D.L., 1989. Geophysical processes influencing the lower continental crust. In: Mereu, R., Mueller, S., Fountain, D. (Eds.), Properties and Processes of Earth's Lower Crust. Geophys. Monogr. Ser. 51, pp. 321–329. AGU, Washington, D.C.
Wallace, P., 2005. Volatiles in subduction zone magmas: concentrations and fluxes based on melt inclusion and volcanic gas data. J. Volcanol. Geotherm. Res. 140, 217–240.
Wan, K., Lin, J., Xia, S., Sun, J., Xu, M., Yang, H., Zhou, Z., Zeng, X., Cao, J., Xu, H., 2019. Deep Seismic Structure across the Southernmost Mariana Trench: implications for Arc Rifting and Plate Hydration. J. Geophys. Res. Solid Earth 124, 4710–4727. https://doi.org/10.1029/2018JB017080.
Wang, X., Zhao, D., Suzuki, H., Li, J., Ruan, A., 2017. Eclogitization of the subducted oceanic crust and its implications for the mechanism of slow earthquakes. Geophys. Res. Lett. 44, 1–8. https://doi.org/10.1002/2017GL074945.
Wang, Z.W., Zhao, D., Chen, X., 2022. Seismic anisotropy and intraslab hydrated faults beneath the NE Japan forearc. Geophys. Res. Lett. 49, e2021GL097266.
Wang, Z.W., Zhao, D., Chen, X., 2023. Fine structure of the subducting slab and the 2022 M7.4 Fukushima-Oki intraslab earthquake. Seismol. Res. Lett. 94, 17–25.
Wessel, P., Luis, J., Uieda, L., Scharroo, R., Wobbe, F., Smith, W., Tian, D., 2019. The generic mapping tools version 6. Geochem. Geophys. Geosyst. 20, 5556–5564. https://doi.org/10.1029/2019GC008515.
Xia, S., Zhao, D., Qiu, X., 2008. Tomographic evidence for the subducting oceanic crust and forearc mantle serpentinization under Kyushu, Japan. Tectonophysics 449, 85–96. https://doi.org/10.1016/j.tecto.2007.12.007.
Xu, W., Peng, X., Stern, R.J., Xu, X., Xu, H., 2023. Challenger deep basalts reveal Indian-type early cretaceous oceanic crust subducting in the southernmost Mariana Trench. Geology 51, 865–869. https://doi.org/10.1130/G51258.1.
Yu, Z., Zhao, D., 2020. Seismic evidence for water transportation in the forearc off Northern Japan. J. Geophys. Res. 125, e2019JB018600 https://doi.org/10.1029/2019JB018600.
Zhang, F., Lin, J., Zhou, Z., Yang, H., Zhan, W., 2018. Intra- and intertrench variations in flexural bending of the Manila, Mariana and global trenches: implications on plate weakening in controlling trench dynamics. Geophys. J. Int. 212, 1429–1449. https://doi.org/10.1093/gji/ggx488.
Zhang, J., Zhang, F., Lin, J., Yang, H., 2021. Yield failure of the subducting plate at the Mariana Trench. Tectonophysics. https://doi.org/10.1016/j.tecto.2021.228944.
Zhang, J., Yang, H., Zhu, G., Chen, H., Zhang, F., Sun, Z., 2023. The effect of along strike variable plate deflection on bending stress and seismicity at the southern Mariana Trench. Tectonophys 850, 229752. https://doi.org/10.1016/j.tecto.2023.229752.
Zhao, D., Hasegawa, A., Horiuchi, S., 1992. Tomographic imaging of P and S wave velocity structure beneath northeastern Japan. J. Geophys. Res. 97, 19909–19928. https://doi.org/10.1029/92JB00603.
Zhao, D., Yanada, T., Hasegawa, A., Umino, N., Wei, W., 2012. Imaging the subducting slabs and mantle upwelling under the Japan Islands. Geophys. J. Int. 190, 816–828. https://doi.org/10.1111/j.1365-246X.2012.05550.x.
Zhao, D., Kitagawa, H., Toyokuni, G., 2015. A water wall in the Tohoku forearc causing large crustal earthquakes. Geophys. J. Int. 200, 149–172. https://doi.org/10.1093/gji/ggu381.
Zhao, D., Katayama, Y., Toyokuni, G., 2022. The Moho, slab and tomography of the East Japan forearc derived from seafloor S-net data. Tectonophysics 837, 229452. https://doi.org/10.1016/j.tecto.2022.229452.
Zhou, Z., Lin, J., 2018. Elasto-plastic deformation and plate weakening due to normal faulting in the subducting plate along the Mariana Trench. Tectonophysics 734, 59–68. https://doi.org/10.1016/j.tecto.2018.04.008.
Zhou, Z., Lin, J., Behn, M.D., Olive, J., 2015. Mechanism for normal faulting in the subducting plate at the Mariana Trench. Geophys. Res. Lett. 42, 4309–4317. https://doi.org/10.1002/2015GL063917.
Zhu, G., Yang, H., Lin, J., Zhou, Z., Xu, M., Sun, J., Wan, K., 2019. Along-strike variation in slab geometry at the southern Mariana subduction zone revealed by seismicity through ocean bottom seismic experiments. Geophys. J. Int. 218, 2122–2135. https://doi.org/10.1093/gji/ggz272.
Zhu, G., Wiens, D., Yang, H., Lin, J., Xu, M., You, Q., 2021. Upper Mantle Hydration Indicated by decreased shear velocity near the Southern Mariana Trench from Rayleigh Wave Tomography. Geophys. Res. Lett. 48, 1–11. https://doi.org/10.1029/2021GL093309.